IEEE Access
Multidisciplinary | Rapid Review | Open Access Journal

Received 7 August 2022, accepted 3 September 2022, date of publication 12 September 2022, date of current version 20 September 2022.

Digital Object Identifier 10.1109/ACCESS.2022.3205733

RESEARCH ARTICLE

Design of a Nonlinear Integral Terminal Sliding Mode Controller for a PEM Fuel Cell Based on a DC-DC Boost Converter

FARZANA AKTER[1], TUSHAR KANTI ROY[1], (Member, IEEE), MD. SHOFIQUL ISLAM[2], ABDULHAMEED FOUAD ALKHATEEB[2], AND MD. ASLAM MOLLAH[1]

[1]Department of Electronics and Telecommunication Engineering, Rajshahi University of Engineering and Technology (RUET), Rajshahi 6204, Bangladesh
[2]Department of Electrical and Computer Engineering, Faculty of Engineering, King Abdulaziz University, Jeddah 21589, Saudi Arabia

Corresponding author: Farzana Akter (farzanaeteruet@gmail.com)

This project was funded by the Deanship of Scientific Research (DSR), King Abdulaziz University, Jeddah, under grant No. (DF-355-135-1441). The authors, therefore, gratefully acknowledge DSR technical and financial support.

ABSTRACT This paper proposes a robust nonlinear controller for a proton exchange membrane fuel cell coupled with a DC-DC boost converter. The key feature is to maintain the desired reference output voltage despite significant disturbances while improving transient stability. In order to do this, a nonlinear robust integral terminal sliding mode controller (ITSMC) is proposed, along with the derivation of the control law, explanation of the reachability analysis, and stability condition. An adapted integral sliding surface is used to capture the dynamics caused by variations in the input voltage and loads. In addition, a modified reaching law is proposed to guarantee the finite time convergence while reducing the chattering. Afterward, the Lyapunov control theory is employed to evaluate the DC-DC boost converter's large-signal stability while guaranteeing the resilience of the proposed controller. Finally, the applicability of the proposed controller is evaluated through comprehensive analyses on both the simulation platform and the real-time processor-in-loop (PIL) platform under various operating conditions, such as the variation in load resistance, reference output voltage, etc. All of the results, when compared to an existing integral terminal sliding mode controller, indicate quick reference tracking capability with reduced overshoots and robustness against disturbances.

INDEX TERMS Control Lyapunov function, integral terminal sliding mode controller, DC-DC boost converter, fuel cell.

I. INTRODUCTION

Due to the modern lifestyle and industrialization, energy consumption is constantly growing. Again, due to a lack of adequate reservoirs and inept or disorderly management, the use of traditional power sources is becoming increasingly constrained. Under this situation, researchers are looking for alternate energy sources to combat air pollution, global warming, and oil depletion [1], [2], [3]. Renewable energy sources (RESs), such as tidal energy, wave energy, wind energy, solar energy, geothermal energy, hydroelectric power and biomass energy, are the solutions to all of these problems [2], [3], [4].

However, fuel cells (FCs) are frequently employed as an alternative energy source because, unlike other RESs, such as wind energy and solar systems, FCs can be deployed everywhere and are climate independent. The proton exchange membrane FC (PEMFC) is chosen for this study over other types of modern FCs because of its high efficiency, high energy density, quicker transient response, rapid start-up, low degradation rate, and ease of maintenance [5], [6], [7]. But this PEMFC is inappropriate owing to the underlying electrochemical and thermodynamic processes, sluggish reaction during transient and instantaneous time, quick voltage drop, and inability to attain maximum load in the case of abrupt

The associate editor coordinating the review of this manuscript and approving it for publication was S. K. Panda.

load demand [8]. Furthermore, unlike batteries, which have a fairly constant output voltage, FCs voltage drops dramatically as the output current increases [9]. As the voltage obtained from the output of a single FC is too low to be employed in practical applications, multiple FCs are linked in series connection to increase the voltage. The cell numbers in the stack of a FC typically ranges from few hundreds to even thousands, depending on the demand of voltage and power. However, such a large number of FCs would reduce the resilience of the stack. Also, the nonlinear features of voltage–current make it difficult for maintaining the stability of output voltage of an FC stack. Therefore, to supply a fixed voltage and raising up the voltage of the FC stack to the required level, a DC–DC converter is necessary. However, due to the non linearity of switching pulses and the non-minimum phase issue that a DC-DC boost converter faces, load voltage stability is a challenging task [10], [11]. To address such a difficulty while improving the performance of the DC-DC boost converter in FC applications, it is required to include a suitable controller with it [12].

The output voltage obtained from a DC-DC boost converter is commonly controlled using proportional-integral-derivative (PID) and a few additional linear controllers that use other approaches [1]. Linear controllers, on the other hand, have a relatively limited operating band since they often employ linearized converter models with a single working point. Furthermore, some of these strategies do not necessitate the use of a model in which the gains are manually or automatically tweaked. As a result, even with a slight step change in the load, these controllers do not achieve the necessary performance [13]. Basically, the switching states of the boost converter give it a nonlinear shape, which makes it difficult to implement in linear controllers [14]. Therefore, nonlinear controllers are essential as these controllers can provide satisfactory results by overcoming all of the constraints of linear controllers. Fuzzy logic controllers [15], feedback linearization controllers [5], backstepping controllers [9], and sliding mode controllers [13] are some examples of nonlinear controllers for FC applications.

For its simplicity and robustness, the data-driven fuzzy-logic controller (FLC) is widely used [15]. In [16], a FLC based on adaptive law is used for a DC-DC step up converter in applications of PEMFCs. However, a significant drawback of FLCs is that the computational requirements have to be incremented for the fuzzy set growth when complex strategies are used during their implementation [5]. Again, the accuracy of the fuzzy system is compromised somehow as the system mostly works on imprecise data and inputs [6].

To overcome the limitations of FLCs, a model-based nonlinear feedback linearization controller (FBLC) is proposed in [7]. However, though the proposed controller can operate over a large range of control points, the expect information about the parameters and explicit model of the system is mandatory to achieve a satisfactory result [8], [9]. To avoid these drawbacks, an adaptive FBLC to handle parametric uncertainties is proposed in [10]. However, the main limitation of this adaptive approach is that it cannot ensure robustness against state-dependent uncertainties [11].

As a result, the nonlinear backstepping controller (NBC) might be utilized to overcome the disadvantages of FBLCs since it can provide satisfactory performance without requiring precise knowledge of the system's parameters, as mentioned in [17]. Ref. [18] discusses a NBC strategy for ensuring the system's dynamic stability. Though this approach can be used to achieve the desired performance, the derivative of a stabilizing function creates some complexities, especially for higher order systems, while overcoming the FBLC's limitations. Furthermore, if the user-defined constants are not appropriately selected, the system's response could be delayed [19].

For mitigating the aforementioned limitations, the sliding mode controller (SMC) is the most operative approach due to its stability, robustness, better energetic response, and high compatibility with the innate switching nature of power converters [20], [21]. Furthermore, as discussed in [22] and [23], an SMC scheme can provide a promising solution for rejecting disturbances and compensating for uncertainty. An SMC approach of dual loop is presented in [24] where the output side voltage is controlled for a fixed input side voltage to establish the asymptotic stability of closed-loop systems. But the controller design is not easy for any dual loop control structure. In association with the FC, a similar type of controller is proposed in [25], but chattering problems are limiting its application practically. To reduce the chattering problem, higher order SMCs are initiated in [26] and [27]. Though these controllers can enhance the output voltage regulation of DC-DC boost converters in the case of FC applications, the tracking error of steady-state cannot be fully diminished. For this reason, a robust SMC scheme is required that not only improves the transient performance of the system but also eliminates the steady-state tracking error. It is well-known that in the SMC technique, it is required to find a control law conditional on a particular sliding surface that changes the dynamics of the system and ensures the asymptotic convergence. But the equilibrium point cannot be gained in a finite time if a conventional reaching law is used, which is challenging for this strategy, Consequently, to solve this challenge and to obtain a finite-time response, a terminal SMC (TSMC) was introduced in [28]. But still, this controller gives a slower response at a distant place from the origin and it terminates with an unbounded control signal due to singularities found. An integral TSMC (ITSMC) can improve the convergence time as well as enhance the chattering reduction stuff and the dynamics of the overall system as discussed in [29] and [30].

Being motivated from the above discussion, the main objective of this paper is to design an ITSMC that is based on a new reaching law to regulate the output voltage of the boost converter. The overall stability and the robustness of the system are proved by the help of control Lyapunov functions (CLFs) at the end of the design procedure. Finally, the proposed controller has been implemented on a MATLAB/SIMULINK platform to assess its performance in

comparison to an existing controller. Moreover, to manifest the effectiveness of the proposed control strategy in practice, the controller performance is also tested on a processor-in-loop (PIL) platform. Basing on the aforementioned analysis, the key offerings of this paper can be described as follows:

- A robust controller is designed by incorporating a time-varying and dynamic sliding surface into this surface to record changes in the system. Furthermore, the related stability certificates give theoretical justification.
- Taking uncertainty, operating state, and circuit parameter changes into consideration, the efficacy of the designed controller is validated.
- Simulation and real-time processor-in-loop (PIL) validations are performed to show efficiency while aiding in the achievement of desired goals in a variety of operating scenarios.
- Due to the application of time-varying reaching laws, it provides improved output voltage tracking accuracy and faster transient responses.

The remaining part of the paper is arranged in the following manner. The system description and its modeling are covered in Section II. Section III represents the suggested controller's design, based on the modeling which is presented in the preceding section. Section-IV is notable for its simulation findings and evaluation of the suggested controller's performance. Finally, section-V represents the concluding words and future scope of this work.

II. SYSTEM DESCRIPTION AND MODELING

The FC and the DC-DC boost converter are the primary units of study, and it is essential to know their operating principles and build a mathematical model for them. Due to the difficulty of modeling chemical processes and the influence of multiple conditions, a common and simple equation of FC model is used. On the basis of the continuous conduction mode, a nonlinear model of the DC-DC boost converter has been built, and all of these are discussed in the following section.

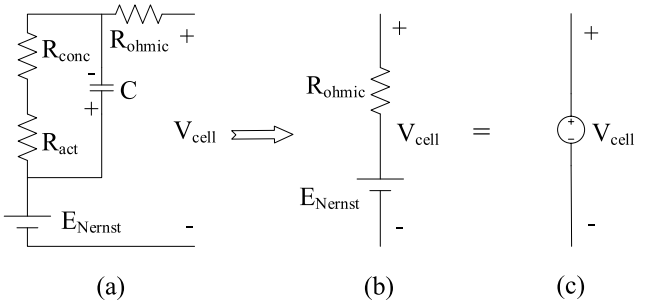

FIGURE 1. Equivalent circuit diagram addressing different types of voltage drops of a PEMFC.

A. MODELING OF THE PEMFC

Basically, the current density of the PEMFC under specific operating circumstances determines its voltage [31]. The current density is frequently used to distinguish between three components: the loss of mass transport, ohmic polarization, and activation polarization. Moreover, before developing the PEMFC model, a few essential presumptions would be taken into account, which are discussed in [32]. According to the assumptions as discussed in [32], the PEMFC equivalent electrical circuit can be represented by Fig. 1 (a). From Fig. 1 (a), the cell voltage of the PEMFC might be written as follows [1], [33]:

$$V_{cell} = E_{Nernst} - \Delta V_{conc} - \Delta V_{ohmic} - \Delta V_{act} \tag{1}$$

where E_{Nernst} stands for the open-circuit reversible voltage, ΔV_{conc} for the concentration-related voltage drop, ΔV_{ohmic} for the ohmic resistance-related voltage drop, and ΔV_{act} for the activation voltage drop, respectively.

At this stage, the open-circuit reversible voltage expression by applying the conventional thermo-dynamical assumptions reported in [34] might be expressed as follows:

$$E_{Nernst} = 1.229 + 4.308 \times 10^{-5}(lnP_{H_2} + lnP_{O_2}) - 8.5 \times 10^{-4}(T - 298.15) \tag{2}$$

where T is the temperature, P_{H_2} is the potential pressure of hydrogen, and P_{O_2} is the potential pressure of oxygen.

The concentration voltage drop, ΔV_{con} can be expressed as follows:

$$\Delta V_{con} = -\frac{R_u T}{nF} ln\left(1 - \frac{I_{FC}}{Ai_L}\right) \tag{3}$$

where F, n, R_u, i_L, I_{FC} and A are used to represent Faraday's constant, number of electrons, constant for the universal gas, limiting current, cell current, and area of the active cell, respectively.

The ohmic voltage drop, ΔV_{ohmic} can be written as follows:

$$\Delta V_{ohmic} = I_{FC} R_{ohmic} \tag{4}$$

where R_{ohmic} is the ohmic resistance. Finally, the activation voltage drop, ΔV_{act} can be expressed as follows [35]:

$$\Delta V_{act} = \epsilon_1 + T\epsilon_2 + T\epsilon_3 lnC_{o_2} + T\epsilon_4 lnI_{FC} \tag{5}$$

where ϵ_i with i=1, 2, 3, 4 represents the cell's parametric coefficient and C_{o_2} is the dissolved oxygen concentration.

At this stage, the FCs output voltage can be calculated by combining all of the preceding equations. However, the single cell's output voltage of a PEMFC is extremely low. So, to boost the output voltage, numerous FCs must be linked to a bipolar plate. Therefore, the stack voltage of a PEMFC can be expressed as follows:

$$V_{FC} = n_{FC} V_{cell} \tag{6}$$

where n_{FC} represents the total number of series connected single FCs.

As discussed in [36], if the operating frequency of the stack reaches to 10 kHz, then R_{act} and R_{conc} can be omitted. Consequently, it could be viewed as a pure and constant resistance, which would then simplify the proposed model to a DC voltage source and an impedance of resistive nature, as illustrated in Fig. 1 (b). For the convenience expression, a voltage source, as indicated in Fig. 1 (c), might be utilized

to replace the structure in Fig. 1 (b). Based on this description, it is clear that the input voltage of a DC-DC boost converter follows the same dynamics as the PEMFC.

An appropriate controller with that of a DC-DC converter might be installed in the real application to increase the PEMFC voltage from lower to a higher and stable DC-bus voltage while staying within the conversion capacity limit. The performance of the current of PEMFC and the DC bus voltage are the key elements of taking into account during this operation. Therefore, the model as displayed in Fig. 1 (c) is worthy of meeting the needs of this study, and basing on this model, the dynamical model of a DC-DC boost converter is presented in the following section.

B. MODELING OF THE DC-DC BOOST CONVERTER

Fig. 2 shows the DC-DC boost converter's comparable circuit diagram. This converter is made up of several parts, including a FC as the input supply voltage, a capacitor (C), an inductor (L), a switch (IGBT), a diode (D), and a load resistor (R). On the basis of pulse width modulation (PWM) approach, the boost converter will be operated for the regulation of output voltage. As a result, the PWM modulated signal must alternate between ON and OFF states to modify the output voltage. The following equation might be used to explain the basic relationship in between the input and the output voltage:

$$V_o = \frac{V_{FC}}{1-d} \tag{7}$$

where d indicates the duty cycle, V_o is the output voltage, and V_{FC} is the input voltage.

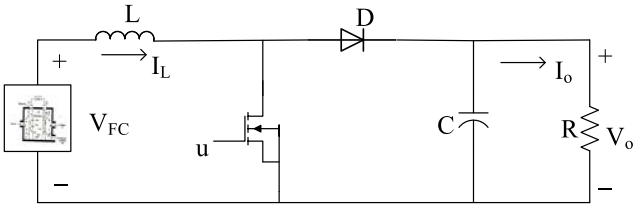

FIGURE 2. Equivalent circuit drawing of a DC DC boost converter with fuel cell as input.

To regulate the output voltage, controlling of duty cycle is indispensable to control the DC-DC boost converter's switching element via a PWM. A dynamical model is required to manage the duty cycle according to the operational condition of the system of DC-DC boost converter, which is explained in the following.

When the switch is OFF:

$$\dot{I_L} = \frac{V_{FC}}{L} - \frac{1}{L}V_o \tag{8}$$

$$\dot{V_o} = \frac{1}{C}I_L - \frac{1}{RC}V_o \tag{9}$$

When the switch is ON:

$$\dot{I_L} = \frac{V_{FC}}{L} \tag{10}$$

$$\dot{V_o} = -\frac{1}{RC}V_o \tag{11}$$

where V_o is the average voltage obtained at the output, I_L is the current flowing through the inductor and $u\epsilon\{0, 1\}$ is the control input of the converter. Therefore, the entire dynamical average model can be represented as follows:

$$\dot{I_L} = \frac{V_{FC}}{L} - \frac{1}{L}(1-u)V_o \tag{12}$$

$$\dot{V_o} = \frac{1}{C}(1-u)I_L - \frac{1}{RC}V_o \tag{13}$$

Eqs. (12), (13) reflect the complete propellant paradigm of a DC-DC boost converter, and the suggested controller will be designed conditioned on this model in the next section.

III. PROPOSED CONTROLLER DESIGN

The control law (u) must be designed to gain quicker transient response, tighter output voltage regulation, and resilience with fewer steady state tracking errors, which is the main goal of this section. The output voltage of the boost converter must be controlled by the tracking of the inductor current. Before continuing further with the design method, the tracking error must be identified. The duty cycle is adjusted to make the output voltage of the converter equal to the reference voltage. To achieve the final control law (u), two steps must be followed according to the controller design technique, which is detailed in the following.

A. SLIDING SURFACE SELECTION

The initial step of this sub-section is to select a stable sliding surface that is aimed to meet the system's requirements. Following the objectives of the design procedure, the tracking error of the inductor current can be expressed as follows:

$$e = I_L - I_{L(ref)} \tag{14}$$

where $I_{L(ref)}$ is the value representing the reference of the inductor current which is calculated using the following formula:

$$I_{L(ref)} = K(V_o - V_{o(ref)}) \tag{15}$$

where K is a proportional gain and $V_{o(ref)}$ is the value representing the reference of the output voltage. The derivative of Eq. (14), using Eq. (12), can be written as:

$$\dot{e} = \frac{V_{FC}}{L} - \frac{1}{L}(1-u)V_o - \dot{I}_{L(ref)} \tag{16}$$

Now, along with the tracking error, the proposed nonlinear integral terminal sliding surface might be defined as follows:

$$S = e + \int (\frac{\alpha}{2}e + \frac{\beta}{2^\gamma}e^\gamma)dt \tag{17}$$

where α, $\beta > 0$, and $0 < \gamma < 1$ are the tuning parameters that are required to control the speed of convergence of the controller. It is worth mentioning that when the frequency is extremely high or infinite, it is feasible to achieve the required control target by simply considering the first term. For a constant frequency, however, this is not practicable since steady-state tracking errors in the inductor current and output voltage will remain. As a result, the integral terminal

term is examined in this study to enhance the steady-state tracking error. Using Eq. (16), the derivative is expressed as follows:

$$\dot{S} = \frac{V_{FC}}{L} - \frac{V_o}{L} + \frac{V_o}{L}u - \dot{I}_{L(ref)} + \frac{\alpha}{2} + \frac{\beta}{2^\gamma}e^\gamma \quad (18)$$

B. DERIVATION OF THE FINAL CONTROL LAW

In the second step, a control law (u) is required to be found to bring the sliding surface into finite time convergence. It is well-known that in the SMC approach, the overall control consists of two parts, which are written as follows:

$$u = u_{eq} + u_{rl} \quad (19)$$

where u_{eq} is the equivalent part of control law and u_{rl} is the reaching law. To obtain u_{eq}, it is obvious to set $\dot{S} = 0$, i.e.,

$$\dot{S} = \frac{V_{FC}}{L} - \frac{V_o}{L} + \frac{V_o}{L}u - \dot{I}_{L(ref)} + \frac{\alpha}{2} + \frac{\beta}{2^\gamma}e^\gamma = 0 \quad (20)$$

From Eq. (20), the equivalent control law can be written as:

$$u_{eq} = \frac{L}{V_o}\left[\frac{V_o}{L} - \frac{V_{FC}}{L} - \dot{I}_{L(ref)} - \frac{\alpha}{2} - \frac{\beta}{2^\gamma}e^\gamma\right] \quad (21)$$

However, to ensure the overall system's stability an improved reaching law u_{rl} is incorporated with the original control law which is written as follows:

$$u_{rl} = -\eta_1|s|^{\sigma_1}sgn(s) - \eta_2|s|^{\sigma_2}sgn(s), \quad (22)$$

where $\eta_1, \eta_2 > 0, \sigma_1 > 1, 0 < \sigma_1 < 1$. Combining Eqs. (19), (21), and (22), the overall control law is

$$u = \frac{L}{V_o}\left[\frac{V_o}{L} - \frac{V_{FC}}{L} - \dot{I}_{L(ref)} - \frac{\alpha}{2} - \frac{\beta}{2^\gamma}e^\gamma - \eta_1|s|^{\sigma_1}sgn(s) - \eta_2|s|^{\sigma_2}sgn(s)\right] \quad (23)$$

Using Eq. (23), Eq. (20) can be rewritten as follows:

$$\dot{S} = -\eta_1|S|^{\sigma_1}sgn(S) - \eta_2|S|^{\sigma_2}sgn(S) \quad (24)$$

C. STABILITY ANALYSIS

For analysing the inclusive stability of the whole system, the following control Lyapunov function (CLF) is chosen. According to this function, a system can be asymptotically stable if $W(S)$ is positive definite and meets the below conditions:

$W(\infty) = \infty$, $W(0) = 0$ and $\dot{W}(S) \leq 0$ Now, the CLF in terms of the sliding surface might be defined as follows:

$$W(S) = \frac{1}{2}S^2 \quad (25)$$

whose derivative is

$$\dot{W}(S) = S\dot{S} \quad (26)$$

Putting the value from Eq. (24), Eq. (26) can be rewritten as follows:

$$\dot{W}(S) = -\eta_1|S|^{\sigma_1+1} - \eta_2|S|^{\sigma_2+1} \quad (27)$$

with $Ssgn(s) = |S|$ From Eq. (27), it can be perceived that the system is steady as $\dot{W}(S)$ is negative definite.

D. REACHABILITY ANALYSIS

Once the system state trajectory reaches the sliding surface, the sliding surface design is such that the system state trajectory will be reaching the equilibrium point in a finite time. Now, the finite time of convergence, t will be determined in this section by considering the nonzero initial state $S(0)$.

By considering the first terms of Eq. (24), it can be detailed as

$$\int_0^{t_1} dt = -\int_{s(0)}^{s(t_1)} \eta_1|S|^{\sigma_1}dS \quad (28)$$

After doing the mathematical manipulation, the required time t_1 can be detailed as follows:

$$t_1 = \frac{1}{\eta_1(\sigma_1 - 1)}[|S(t_1)|^{1-\sigma_1} - |S(0)|^{1-\sigma_1}] \quad (29)$$

Similarly, for the second term of Eq. (24), the required time t_2 can be detailed as follows:

$$t_2 = \frac{1}{\eta_2(\sigma_2 - 1)}[|S(t_2)|^{1-\sigma_2} - |S(0)|^{1-\sigma_2}] \quad (30)$$

Now, by combining Eqs. (29) and (30), the total finite time of convergence (t) is expressed as follows:

$$t = \frac{1}{\eta_1(\sigma_1 - 1)}[|S(t_1)|^{1-\sigma_1} - |S(0)|^{1-\sigma_1}] + \frac{1}{\eta_2(\sigma_2 - 1)}[|S(t_2)|^{1-\sigma_2} - |S(0)|^{1-\sigma_2}] \quad (31)$$

Thus, from Eq. (31), it is confirmed that both the tracking error and the derivative of it will converge to zero in a finite time. In the next section, the efficacy of the designed controller is analyzed.

IV. SIMULATION RESULTS AND PERFORMANCE EVALUATION

This section includes both simulation and experimental processor-in-loop (PIL) studies to evaluate the efficacy of the designed controller. The simulation investigation has been carried out on the MATLAB/Simulink platform. The implementation block diagram in Fig. 3 depicts the overall simulation structure in which the FC output is provided as input to the DC-DC boost converter. Afterward, the sliding surface is determined using the system's output. Finally, the actual control signal is computed and supplied back via the PWM to the DC-DC boost converter switch. The simulation settings for the designed nonlinear controller are selected by prioritizing future prototype development while keeping practical situations in mind. As a result, the system and controller parameters utilized in this simulation are provided in Table 1 and Table 2 respectively. For convenience, the controller parameters are chosen basing on the trial and error methodology to fulfil the cherished control objectives.

By using these parameters, the final control law (u) is evaluated that is to be applied to the converter's switch through a pulse width modulator (PWM) where 100 kHz is chosen as the switching frequency. To test the ability of output voltage tracking and to assess the proposed controller's performance,

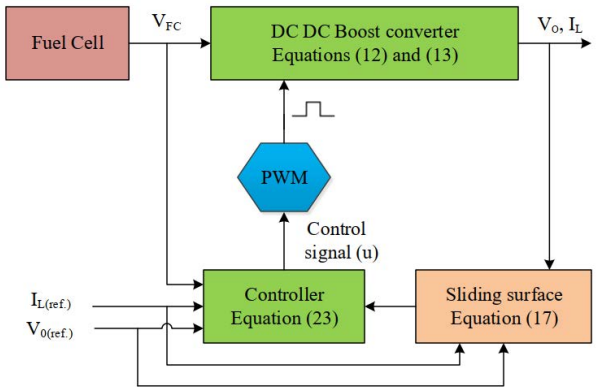

FIGURE 3. Schematic drawing for implementation of the proposed controller.

TABLE 1. System parameters.

Variables	Description	Values
C	Capacitance (μF)	100
f_s	Switching frequency (kHz)	100
L	Inductance (H)	0.001
R	Resistance (Ω)	130/140
V_{FC}	Output voltage of the FC (V)	41/31
V_{ref}	Reference voltage (V)	60/70/55

TABLE 2. Control parameters.

Variables	Values
Proposed controller	
α	500000
β	1000
γ	0.3
η_1	600
η_2	600
σ_1	1.01
σ_2	0.3
Existing controller	
η	5
k_1	0.0000025
k_2	1000000
p/q	9/5

it is compared with an existing integral terminal sliding mode controller (ITSMC) as presented in [29] by considering three cases. These cases are listed as follows:

Case I: Controller performance under the variation in load resistance.

Case II: Controller performance under the variation in the input supply voltage.

Case III: Controller performance under the variation in the reference output voltage.

The above mentioned case studies were conducted to understand the robustness of the designed controller in applications of proton exchange membrane fuel cells (PEMFC). The cases are elaborately discussed in the following.

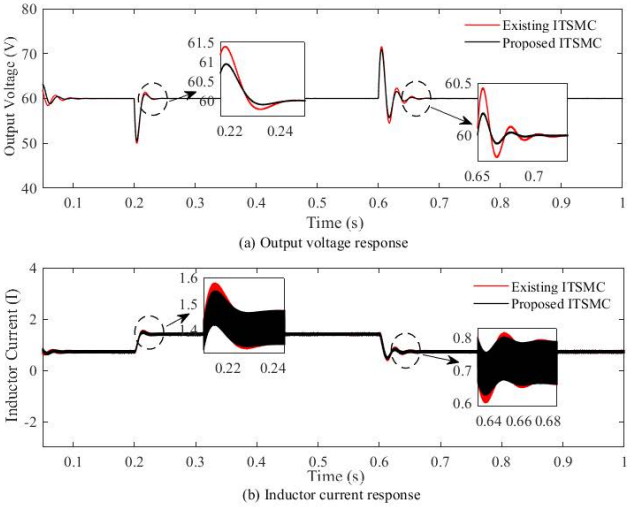

FIGURE 4. Various response curves for case-I.

A. CASE I: CONTROLLER PERFORMANCE UNDER THE VARIATION IN LOAD RESISTANCE

In the study of this case, the performance of the designed controller is validated by varying the load resistance. The load resistance is varied according to the following mathematical equation:

$$R_{load} = \begin{cases} 130; & 0 \le t < 0.2 \\ 140; & 0.2 \le t < 0.6 \\ 130; & 0.6 \le t < 1 \end{cases}$$

The corresponding response is presented in Fig. 4. From the above shown diagrams, it can be stated that the first transient response occurs at a time period of 0.2 s and the following occurs at a time period of 0.6 s. The red-colored curve indicates the controller performance of the existing one, while the black-colored curve indicates the performance measure of the proposed controller. From Fig. 4, it can be seen that the initial evaluation has started from a time period of 0.05 s as priority is given to the two transient conditions and has ended after 1 s. From Fig. 4 (a), it is also observed that the proposed controller exhibits an overshoot of 1.57%, an undershoot of 15.75%, and a settling time of 0.041s, while the existing one shows an overshoot of 2.33%, an undershoot of 16.67%, and a settling time of 0.043 s at an initial transient time of 0.2 s. Similarly, an overshoot, undershoot, and settling time of 18.17%, 7.13%, and 0.096s, respectively, is observed for the proposed controller at a second transient time of 0.6 s, while 19.25%, 9.13%, and 0.122 s of overshoot, undershoot, and settling time are observed, respectively for the existing controller. Fig. 4 (b) represents the inductor current response versus time (s). This curve also represents the same type of result at transient conditions as that of the response curve of output voltage. So, the above mentioned observations clearly shows the supremacy of the proposed controller design with respect to the existing one. Table 3 is representing the quantitative analysis of the voltage for Case I.

TABLE 3. Quantitative analysis of voltage for Case I.

Time to switch the operating point (s)	Controllers	Peak Value	Over shoot (%)	Lower Value	Under shoot (%)	Settling time (s)
T=0.2	Existing	61.40	2.33	50.00	16.67	0.043
	Proposed	60.94	1.57	50.55	15.75	0.041
T=0.6	Existing	71.55	19.25	54.52	9.13	0.122
	Proposed	70.90	18.17	55.72	7.13	0.096

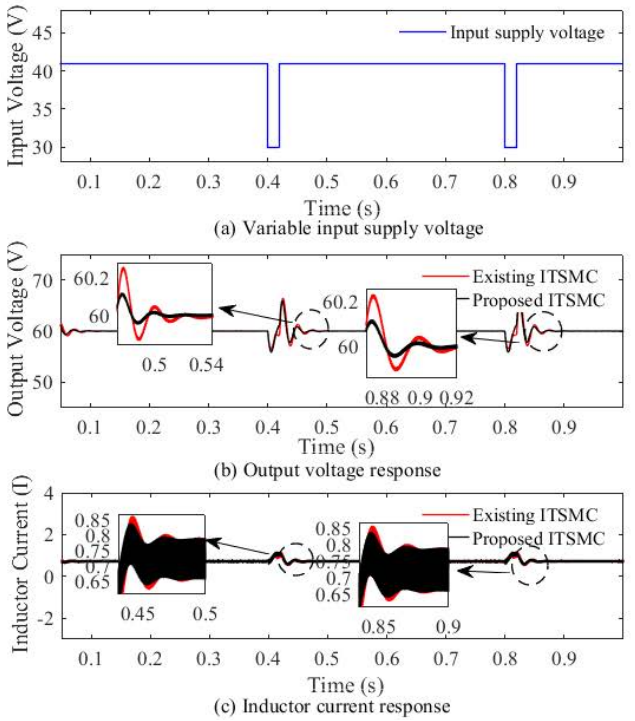

FIGURE 5. Various response curves for case-II.

B. CASE II: CONTROLLER PERFORMANCE UNDER THE VARIATION IN THE INPUT SUPPLY VOLTAGE

In the study of this case, the performance of the designed controller is validated by varying the input supply voltage. Actually, the input supply voltage that is proposed in this work is from the FC output voltage. The characteristics of a FC show a lower limit of voltage that is approximately 0.5 V, beyond which the FC voltage starts to decreases very sharply with an increase in current [37]. Due to various thermodynamic reactions taking place inside the FC, sometimes the rate of reaction is greater and sometimes less because the output obtained from the FC is also variable [29]. For this reason, the simulation is validated for variable input supply voltage to show the real scenario of the FC. Fig. 5 (a) depicts the curve of a variable input supply voltage where the initial supply is at 41 V, the input supply is replaced by 30 V after 0.4 s, and the previous condition is regained after some time. The same phenomenon is observed for the second transient time of 0.8 s.

Fig. 5 (b) depicts the output voltage response with time (s), and Table 4 shows the quantitative analysis of voltage for Case II. It is seen from the table that the proposed controller exhibits overshoot of 9.8%, undershoot of 4.92%, and

TABLE 4. Quantitative analysis of voltage for Case II.

Time to switch the operating point (s)	Controllers	Peak Value	Over shoot (%)	Lower Value	Under shoot (%)	Settling time (s)
T=0.4	Existing	66.42	10.7	57.04	4.93	0.145
	Proposed	65.88	9.8	57.05	4.92	0.104
T=0.8	Existing	66.33	10.55	57.14	4.77	0.12
	Proposed	65.86	9.77	57.76	3.73	0.093

a settling time of 0.104 s at the initial transient response time of 0.4 s, whereas the existing controller exhibits 10.7%, 4.93%, and 0.145 s of overshoot, undershoot, and settling time, respectively. During the second transient response of 0.8 s, like the previous response time, the proposed controller scheme exhibits overshoot, undershoot, and settling time of 9.77%, 3.73%, and 0.093 s, respectively, and the existing controller curve exhibits 10.55%, 4.77%, and 0.12 s of overshoot, undershoot, and settling time, respectively. Hence, the designed controller shows better tracking performance in comparison to the existing controller. Similarly, the inductor current response versus time curve shown in Fig. 5 (c) demonstrates that the proposed controller shows it's supremacy over the existing controller in terms of overshoot, undershoot, and settling time.

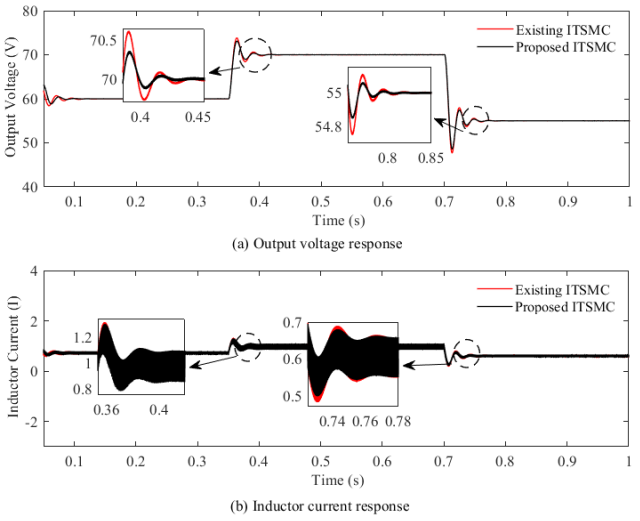

FIGURE 6. Various response curves for case-III.

C. CASE III: CONTROLLER PERFORMANCE UNDER THE VARIATION IN THE REFERENCE OUTPUT VOLTAGE

In this case study, at an initial transient response time of 0.35 s, the reference voltage starts to increase from 60 V to 70 V and so on. But, during the second transient response time of 0.7 s, the reference voltage steps down to 55 V from 70 V and goes on. The following mathematical expression can clearly demonstrate the above statement:

$$V_{o(ref)} = \begin{cases} 60; & 0 \le t < 0.35 \\ 70; & 0.35 \le t < 0.7 \\ 55; & 0.7 \le t < 1 \end{cases}$$

Fig. 6 (a) represents the output voltage response versus time (s) curve for understanding the controller performance with variable reference output voltage. The quantitative analysis of voltage for Case III is shown in Table 5.

TABLE 5. Quantitative analysis of voltage for Case III.

Time to switch the operating point (s)	Controllers	Peak Value	Over shoot (%)	Lower Value	Under shoot (%)	Settling time (s)
T=0.35	Existing	73.80	5.43	68.41	2.27	0.114
	Proposed	73.10	4.43	68.96	1.49	0.075
T=0.7	Existing	57.96	5.38	47.72	13.24	0.15
	Proposed	57.42	4.40	48.58	11.67	0.089

From the above table, it is observed that the designed controller gives an overshoot of 4.43%, an undershoot of 1.49% and a settling time of 0.075 s during the first transient response time of 0.35 s, whereas the existing ITSMC exhibits an overshoot of 5.43%, an undershoot of 2.27% and a settling time of 0.114s. Similarly, during the second transient response of time 0.7 s, the overshoot, undershoot, and settling time are 4.4%, 11.67%, and 0.089 s, respectively, for the designed controller, while the existing controller exhibits an overshoot of 5.38%, an undershoot of 13.24%, and a settling time of 0.15 s. So, in conclusion it is seen that the designed controller outperforms the existing controller.

Fig. 6 (b) depicts the inductor current versus time (s) curve for the same scenario and exhibits a similar type of output response. Thus, it can be stated that the design is capable of providing better performance as compared to the existing controller.

D. ANALYSIS OF COMPARATIVE PERFORMANCE USING INTEGRAL ERROR-PERFORMANCE INDICES

Integrals of error-based performance indices such as the integral of absolute error (IAE), integral time absolute error (ITAE), integral square error (ISE) and integral time square error (ITSE) are used to compare the proposed and existing controllers. All four indices are calculated for both controllers and presented in Table 6, which clearly shows that the designed controller has substantially lower values than the existing controller. The following section covers the performance evaluation of the PIL platform.

E. PIL VALIDATIONS

The PIL platform is used to support the findings of theoretical and simulation investigations. The control input is directed to a real-time processor on this platform through a PIL block

TABLE 6. Quantitative analysis of error for all the cases.

Cases	Controllers	IAE $\int_0^\infty \lvert e(t)\rvert dt$	ITAE $\int_0^\infty t\lvert e(t)\rvert dt$	ISE $\int_0^\infty e^2(t)dt$	ITSE $\int_0^\infty e^2(t)dt$
Case I	Existing	0.273	0.119	1.474	0.659
	Proposed	0.248	0.107	1.352	0.605
Case II	Existing	0.294	0.174	0.969	0.598
	Proposed	0.262	0.157	0.815	0.505
Case III	Existing	0.292	0.158	1.518	0.899
	Proposed	0.254	0.137	1.458	0.869

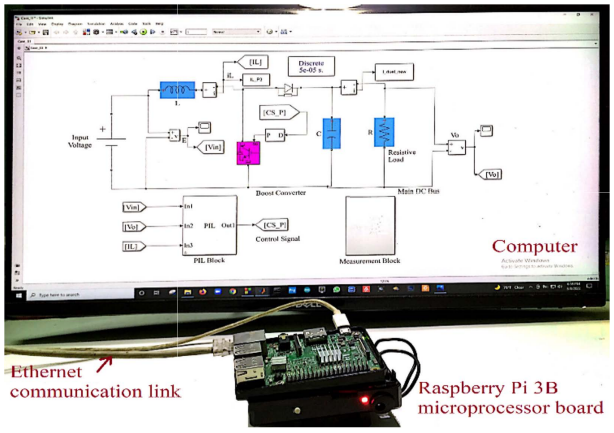

FIGURE 7. Experimental set up of PIL.

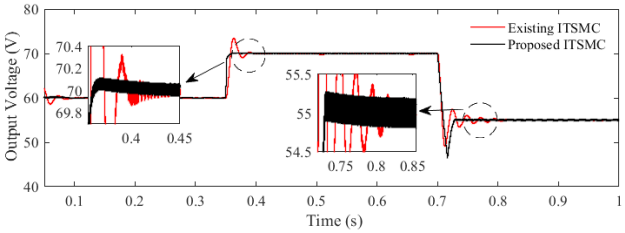

FIGURE 8. Output voltage response of controller for variable reference voltage during PIL validation.

(as illustrated in Fig. 7). (Rasberry Pi 3B Quad-Core 64-bit Microprocessor Development Board). The control signal generated from the processor is feedback to the Simulink platform, which indicates that the control signal is generated on a real-time platform where an analog signal is received by the microprocessor board. Thus, a suitable control signal is generated on the development board by a combination of reference values created in real time on the platform and actual board values. This analog control signal is then transferred as the input of the switching pulse generator. Fig. 7 depicts an Ethernet cable that sends and receives data between the simulator and the processor. It is noteworthy that a similar system as that of the simulation study is used here with the only difference being the implementation of the controller in the real-time environment. Here, analysis is performed to show the robustness of both the controllers under the variations of reference output voltage as described in case-III of the earlier discussed subsection.

The output voltage response curve in Fig. 8 indicates that in the PIL platform, the proposed ITSMC controller has neither overshoot or undershoot and has a faster settling time than the existing controller when both transient times of 0.35 s and 0.7 s are taken into account. This experimental setup and approach can demonstrate the developed controller's real-time performance improvement in all circumstances. Finally, the proposed controller provides a better dynamic response than the existing one.

V. CONCLUSION

In this paper, a nonlinear robust integral terminal sliding mode controller (ITSMC) for a DC-DC boost converter

in applications of proton exchange membrane fuel cells is designed. An average mathematical model of the boost converter is used for designing the proposed controller, with the control purpose of monitoring the reference output voltage. The final control law is considered to eliminate the steady state tracking error while producing a quicker transient response using an integral terminal based sliding surface, as presented in this paper. The application of control Lyapunov functions confirms the overall system's stability. MATLAB/Simulink and processor in loop are chosen as the platforms to implement the designed controller to ensure its effectiveness by varying the load resistance, the input supply voltage and the reference output voltage. In terms of dynamic stability and steady state tracking error, quicker transient response, overshoot, undershoot, and settling time, simulation results clearly indicate that the designed controller outperforms the existing integral terminal sliding mode controller. The effects of external disturbances and model perturbations are not taken into account by the mathematical model. Therefore, by include these implications in the model, future work will further enhance the controller design process. Furthermore, the designed controller has not yet been implemented in the real physical system, despite being deployed in the processor-in-loop platform. So, the designed controller can be implemented in a practical prototype system built in a lab in the future to confirm its applicability.

ACKNOWLEDGMENT

This project was funded by the Deanship of Scientific Research (DSR), King Abdulaziz University, Jeddah, under grant No. (DF-355-135-1441). The authors, therefore, gratefully acknowledge DSR technical and financial support.

REFERENCES

[1] S. Ahmadi, S. Abdi, and M. Kakavand, "Maximum power point tracking of a proton exchange membrane fuel cell system using PSO-PID controller," *Int. J. Hydrogen Energy*, vol. 42, no. 32, pp. 20430–20443, Aug. 2017.

[2] T. K. Roy and M. A. Mahmud, "Active power control of three-phase grid-connected solar PV systems using a robust nonlinear adaptive backstepping approach," *Sol. Energy*, vol. 153, pp. 64–76, Sep. 2017.

[3] T. K. Roy and M. A. Mahmud, "Dynamic stability analysis of hybrid islanded DC microgrids using a nonlinear backstepping approach," *IEEE Syst. J.*, vol. 12, no. 4, pp. 3120–3130, Dec. 2018.

[4] T. K. Roy, M. A. Mahmud, A. M. T. Oo, M. E. Haque, K. M. Muttaqi, and N. Mendis, "Nonlinear adaptive backstepping controller design for islanded DC microgrids," *IEEE Trans. Ind. Appl.*, vol. 54, no. 3, pp. 2857–2873, May/Jun. 2018.

[5] I. M. Safwat, X. Wu, X. Zhao, and W. Li, "Adaptive fuzzy logic control of boost converter fed by stand-alone PEM fuel cell stack," in *Proc. IEEE Transp. Electrific. Conf. Expo, Asia–Pacific (ITEC Asia–Pacific)*, Aug. 2017, pp. 1–6.

[6] A. Harrag and S. Messalti, "How fuzzy logic can improve PEM fuel cell MPPT performances?" *Int. J. Hydrogen Energy*, vol. 43, no. 1, pp. 537–550, Jan. 2018.

[7] W. K. Na and B. Gou, "Feedback-linearization-based nonlinear control for PEM fuel cells," *IEEE Trans. Energy Convers.*, vol. 23, no. 1, pp. 179–190, Mar. 2008.

[8] S. M. Mohiuddin, M. A. Mahmud, A. M. O. Haruni, and H. R. Pota, "Design and implementation of partial feedback linearizing controller for grid-connected fuel cell systems," *Int. J. Electr. Power Energy Syst.*, vol. 93, pp. 414–425, Dec. 2017.

[9] A. Abaspour, N. T. Parsa, and M. Sadeghi, "A new feedback linearization-NSGA-II based control design for PEM fuel cell," *Int. J. Comput. Appl.*, vol. 97, no. 10, pp. 25–32, Jul. 2014.

[10] A. Abbaspour, A. Khalilnejad, and Z. Chen, "Robust adaptive neural network control for PEM fuel cell," *Int. J. Hydrogen Energy*, vol. 41, no. 44, pp. 20385–20395, 2016.

[11] T. K. Roy, M. F. Pervej, S. Rahman, and F. K. Tumpa, "Nonlinear adaptive controller design for PWM based DC-DC boost converters using bankstepping control scheme," in *Proc. 5th Int. Conf. Informat., Electron. Vis. (ICIEV)*, May 2016, pp. 608–613.

[12] M. A. Mahmud, T. K. Roy, S. Saha, M. E. Haque, and H. R. Pota, "Robust nonlinear adaptive feedback linearizing decentralized controller design for islanded DC microgrids," *IEEE Trans. Ind. Appl.*, vol. 55, no. 5, pp. 5343–5352, Sep. 2019.

[13] T. K. Roy, M. A. Mahmud, and A. M. T. Oo, "Robust adaptive backstepping excitation controller design for higher-order models of synchronous generators in multimachine power systems," *IEEE Trans. Power Syst.*, vol. 34, no. 1, pp. 40–51, Jan. 2019.

[14] V. M. García, M. Serra, J. Llorca, and J. Riera, "Design of linear controllers applied to an ethanol steam reformer for PEM fuel cell applications," *Int. J. Hydrogen Energy*, vol. 38, no. 18, pp. 7640–7646, Jun. 2013.

[15] A. B. Kebede and G. B. Worku, "Robust DC-DC boost converter control for integration of fuel cell with renewable energy sources," *Int. J. Eng. Res. Afr.*, vol. 49, pp. 68–83, Jun. 2020.

[16] N. E. Benchouia, A. Derghal, B. Mahmah, B. Madi, L. Khochemane, and E. H. Aoul, "An adaptive fuzzy logic controller (AFLC) for PEMFC fuel cell," *Int. J. Hydrog. Energy.*, vol. 40, no. 39, pp. 13806–13819, Oct. 2015.

[17] X. Hao, I. Salhi, S. Laghrouche, Y. Ait-Amirat, and A. Djerdir, "Backstepping supertwisting control of four-phase interleaved boost converter for PEM fuel cell," *IEEE Trans. Power Electron.*, vol. 37, no. 7, pp. 7858–7870, Jul. 2022.

[18] R. Patel and D. Deb, "Parametrized control-oriented mathematical model and adaptive backstepping control of a single chamber single population microbial fuel cell," *J. Power Sources*, vol. 396, pp. 599–605, Aug. 2018.

[19] M. Derbeli, M. Farhat, O. Barambones, and L. Sbita, "Control of PEM fuel cell power system using sliding mode and super-twisting algorithms," *Int. J. Hydrogen Energy*, vol. 42, no. 13, pp. 8833–8844, Mar. 2017.

[20] T. Ahmed, A. Waqar, R. M. Elavarasan, J. Imtiaz, M. Premkumar, and U. Subramaniam, "Analysis of fractional order sliding mode control in a D-STATCOM integrated power distribution system," *IEEE Access*, vol. 9, pp. 70337–70352, 2021.

[21] D. Menaga and V. Sankaranarayanan, "Performance comparison for grid connected photovoltaic system using sliding mode control," *J. King Saud Univ.-Eng. Sci.*, vol. 33, no. 4, pp. 276–283, May 2021.

[22] W. Garcia-Gabin, F. Dorado, and C. Bordons, "Real-time implementation of a sliding mode controller for air supply on a PEM fuel cell," *J. Process Control*, vol. 20, no. 3, pp. 325–336, 2010.

[23] D. Menaga, M. Premkumar, R. Sowmya, and S. Narasimman, "Design of nonlinear uncertainty controller for grid-tied solar photovoltaic system using sliding mode control," *J. Assoc. Energy Eng.*, vol. 117, p. 481, Jul. 2020.

[24] R. Saadi, O. Kraa, M. Y. Ayad, M. Becherif, H. Ghodbane, M. Bahri, and A. Aboubou, "Dual loop controllers using PI, sliding mode and flatness controls applied to low voltage converters for fuel cell applications," *Int. J. Hydrogen Energy*, vol. 41, no. 42, pp. 19154–19163, Nov. 2016.

[25] M. R. Islam, M. A. Hossain, J. Hasan, T. K. Roy, and M. A. H. Sadi, "Double integral sliding mode controller based bridge-type flux-coupling non-superconducting fault current limiter to protect DFIG-based multi-machine power system under transient-state," *Int. J. Electr. Power Energy Syst.*, vol. 142, Nov. 2022, Art. no. 108271.

[26] Y. Wu, Y. Huangfu, R. Ma, A. Ravey, and D. Chrenko, "A strong robust DC-DC converter of all-digital high-order sliding mode control for fuel cell power applications," *J. Power Sources*, vol. 413, pp. 222–232, Feb. 2019.

[27] M. Derbeli, O. Barambones, M. Farhat, J. A. Ramos-Hernanz, and L. Sbita, "Robust high order sliding mode control for performance improvement of PEM fuel cell power systems," *Int. J. Hydrogen Energy*, vol. 45, no. 53, pp. 29222–29234, Oct. 2020.

[28] H. Armghan, M. Yang, A. Armghan, N. Ali, M. Q. Wang, and I. Ahmad, "Design of integral terminal sliding mode controller for the hybrid AC/DC microgrids involving renewables and energy storage systems," *Int. J. Electr. Power Energy Syst.*, vol. 119, Jul. 2020, Art. no. 105857.

[29] C. Napole, M. Derbeli, and O. Barambones, "A global integral terminal sliding mode control based on a novel reaching law for a proton exchange membrane fuel cell system," *Appl. Energy*, vol. 301, Nov. 2021, Art. no. 117473.

[30] T. K. Roy, M. A. H. Pramanik, and S. K. Ghosh, "Design of an integral terminal-based sliding mode controller for PV and BESS-based DC microgrids," *Energy Nexus*, vol. 7, Sep. 2022, Art. no. 100130.
[31] X. Chen, J. Xu, C. Yang, Y. Fang, W. Li, Y. Zhang, Z. Wan, and X. Wang, "Thermodynamic and economic study of PEMFC stack considering degradation characteristic," *Energy Convers. Manag.*, vol. 235, May 2021, Art. no. 114016.
[32] S.-W. Tsai and Y.-S. Chen, "A mathematical model to study the energy efficiency of a proton exchange membrane fuel cell with a dead-ended anode," *Appl. Energy*, vol. 188, pp. 151–159, Feb. 2017.
[33] M. Derbeli, O. Barambones, and L. Sbita, "A robust maximum power point tracking control method for a PEM fuel cell power system," *Appl. Sci.*, vol. 8, no. 12, p. 2449, Dec. 2018.
[34] E. W. Saeed and E. G. Warkozek, "Modeling and analysis of renewable PEM fuel cell system," *Energy Proc.*, vol. 74, pp. 87–101, Aug. 2015.
[35] J. Y. Fam, S. Y. Wong, H. B. M. Basri, M. O. Abdullah, K. B. Lias, and S. Mekhilef, "Predictive maximum power point tracking for proton exchange membrane fuel cell system," *IEEE Access*, vol. 9, pp. 157384–157397, 2021.
[36] A. De Bernardinis, M.-C. Péra, J. Garnier, D. Hissel, G. Coquery, and J.-M. Kauffmann, "Fuel cells multi-stack power architectures and experimental validation of 1 kW parallel twin stack PEFC generator based on high frequency magnetic coupling dedicated to on board power unit," *Energy Convers. Manage.*, vol. 49, no. 8, pp. 2367–2383, 2008.
[37] A. Hajizadeh and M. A. Golkar, "Power flow control of grid-connected fuel cell distributed generation systems," *J. Electr. Eng. Technol.*, vol. 3, no. 2, pp. 143–151, Jun. 2008.

FARZANA AKTER received the B.Sc. degree in electronics and telecommunication engineering (ETE). She is currently pursuing the M.Sc. degree in electronics and telecommunication engineering (ETE). She is currently a Lecturer with the Department of Electronics and Telecommunication Engineering (ETE), Rajshahi University of Engineering and Technology (RUET). Her research interests include biomedical engineering and controller design for renewable energy sources.

TUSHAR KANTI ROY (Member, IEEE) received the B.Sc. degree in electrical and electronic engineering from the Rajshahi University of Engineering and Technology, Rajshahi, Bangladesh, in 2008, and the M.E. (research) degree in electrical engineering from the University of New South Wales, Canberra, ACT, Australia, in 2012, and the Ph.D. degree in electrical engineering from Deakin University, Waurn Ponds, VIC, Australia, in 2019. He is currently working as an Associate Professor with the Department of Electronics and Telecommunication Engineering, Rajshahi University of Engineering and Technology. His research interests include nonlinear control theory and applications, excitation control, microgrid, renewable energy, and power electronics.

MD. SHOFIQUL ISLAM received the B.Sc. and M.Sc. degrees in electrical and electronic engineering from the Bangladesh University of Engineering and Technology, Bangladesh, in 1999 and 2002, respectively, and the Ph.D. degree in electronic and information engineering from the Toyohashi University of Technology, Japan, in 2007.

He is currently working as an Associate Professor with the Department of Electrical and Computer Engineering, King Abdulaziz University, Saudi Arabia. He published 45 papers in journals and conferences. His research interests include modeling and simulation of MOSFET, tunnel FET, GNR FET; analytical modeling of organic and Si-based solar cells; design and numerical simulation of plasmonic sensors; design, fabrication and performance analysis of special shaped MEMS, NEMS structures for sensor applications; fabrication of vertical needle-shaped electronic devices for bio-sensing; design of electronic circuits for different applications; and mathematical solutions of the problems in engineering. He has the experience of theoretical research works as well as the experience of practical works in clean-room environment for fabricating electronic devices, sensors, and MEMs structures. He received the Best Paper Award from Asia–Pacific Conference of Transducers and Micro-Nano Technology (APCOT), Singapore.

ABDULHAMEED FOUAD ALKHATEEB received the B.Sc. degree in electrical engineering (electronics and communication) from King Abdulaziz University, Jeddah, Saudi Arabia, in 1987, the M.Sc. degree in bioengineering from the University of Michigan, Ann Arbor, MI, USA, in 1992, and the Ph.D. degree in bioengineering from Pennsylvania State University, USA, in 1997.

He is currently an Associate Professor of electrical and biomedical engineering with the Department of Electrical and Computer Engineering, King Abdulaziz University. He held many positions and CTO and CBO. He is an inventor receiving seven patents in the past two years alone from the U.S. patent Office and translated several books. He has also published many articles in ISI journals some of which are Q1 journals. His research interests include wavelet, signal processing, ECG, EEG and EMG signal detection and analysis, sensors, fuzzy logic, solid state fabrication and design, control systems, clinical engineering management, electrophysiology, brain–computer interface, and surgical simulations and VR/AR systems.

Dr. Alkhateeb his academic achievements, he has wide hands-on experience in designing hospitals with the latest FGI standards, Medical Equipment Planning, setting up and running clinical engineering departments in hospital, JCI, and CBAHI accreditation to name a few.

MD. ASLAM MOLLAH received the B.Sc. degree in electronics and telecommunication engineering (ETE) and the M.Sc. degree in electrical and electronic engineering (EEE) from the Rajshahi University of Engineering and Technology. He is currently an Assistant Professor of electronics and telecommunication engineering at the Rajshahi University of Engineering and Technology. He published 21 peer-reviewed articles and actively reviews for IEEE JOURNAL OF LIGHTWAVE TECHNOLOGY, *Optics Express*, *Journal of the Optical Society of America B* (JOSA B), *Applied Optics*, *OSA Continuum*, *ACS Applied Nano Materials*, *Optical Fiber Technology*, and *Optik*. His research interests include optical fiber communication, PCF based terahertz waveguides, terahertz sensors, and surface plasmon resonance biosensors.